AGU PUBLICATIONS

JGR

Journal of Geophysical Research: Oceans

RESEARCH ARTICLE

10.1002/2016JC012281

Key Points:
- Ship-based air-sea fluxes in the Antarctic Marginal Ice Zone (MIZ) are estimated using algorithms specifically tuned for sea ice
- Air-sea turbulent exchanges in the MIZ varied greatly with season, both in location and in physical processes
- Compared to the sub-Antarctic region, seasonal changes of turbulent heat fluxes dominate the surface heat budget in the MIZ

Correspondence to:
L. Yu,
lyu@whoi.edu

Citation:
Yu, L., X. Jin, E. W. Schulz, and S. A. Josey (2017), Air-sea interaction regimes in the sub-Antarctic Southern Ocean and Antarctic marginal ice zone revealed by icebreaker measurements, *J. Geophys. Res. Oceans*, *122*, 6547–6564, doi:10.1002/2016JC012281.

Received 25 AUG 2016
Accepted 20 JUN 2017
Accepted article online 5 JUL 2017
Published online 23 AUG 2017

Air-sea interaction regimes in the sub-Antarctic Southern Ocean and Antarctic marginal ice zone revealed by icebreaker measurements

Lisan Yu[1], Xiangze Jin[1], Eric W. Schulz[2], and Simon A. Josey[3]

[1]Department of Physical Oceanography, Woods Hole Oceanographic Institution, Woods Hole, Massachusetts, USA, [2]Centre for Australian Weather and Climate Research, Australian Bureau of Meteorology, Melbourne, Victoria, Australia, [3]National Oceanography Centre, Southampton, UK

Abstract This study analyzed shipboard air-sea measurements acquired by the icebreaker *Aurora Australis* during its off-winter operation in December 2010 to May 2012. Mean conditions over 7 months (October–April) were compiled from a total of 22 ship tracks. The icebreaker traversed the water between Hobart, Tasmania, and the Antarctic continent, providing valuable in situ insight into two dynamically important, yet poorly sampled, regimes: the sub-Antarctic Southern Ocean and the Antarctic marginal ice zone (MIZ) in the Indian Ocean sector. The transition from the open water to the ice-covered surface creates sharp changes in albedo, surface roughness, and air temperature, leading to consequential effects on air-sea variables and fluxes. Major effort was made to estimate the air-sea fluxes in the MIZ using the bulk flux algorithms that are tuned specifically for the sea-ice effects, while computing the fluxes over the sub-Antarctic section using the COARE3.0 algorithm. The study evidenced strong sea-ice modulations on winds, with the southerly airflow showing deceleration (convergence) in the MIZ and acceleration (divergence) when moving away from the MIZ. Marked seasonal variations in heat exchanges between the atmosphere and the ice margin were noted. The monotonic increase in turbulent latent and sensible heat fluxes after summer turned the MIZ quickly into a heat loss regime, while at the same time the sub-Antarctic surface water continued to receive heat from the atmosphere. The drastic increase in turbulent heat loss in the MIZ contrasted sharply to the nonsignificant and seasonally invariant turbulent heat loss over the sub-Antarctic open water.

Plain Language Summary The icebreaker Aurora Australis is a research and supply vessel that is regularly chartered by the Australian Antarctic Division during the southern summer to operate in waters between Hobart, Tasmania, and Antarctica. The vessel serves as the main lifeline to three permanent research stations on the Antarctic continents and provide critical support for Australia's Southern Ocean research operation. Automated meteorological measurement systems are deployed onboard the vessel, providing routine observations of wind, air and sea temperature, humidity, pressure, precipitation and long- and short-wave radiation. Two climatically important regimes are sampled as the icebreaker sails across the sub-Antarctic Southern Ocean and traverses the marginal region of the East Antarctic continent. One regime is the Antarctic Circumpolar Current (ACC) system where strong westerly winds are featured. The other is the Antarctic seasonal marginal ice zone (MIZ), i.e., the narrow transition zone that connects the ice-free sub-Antarctic with the Antarctic ice-covered regime. Observing the remote Southern Ocean has been historically challenging due to the cost realities and logistical difficulties. The shipboard and near-surface meteorological measurements offer a rare and valuable opportunity for gaining an in situ insight into the air-sea heat and momentum exchange in two poorly sampled yet dynamically important regimes.

1. Introduction

The icebreaker *Aurora Australis* is a research and supply vessel that is regularly chartered by the Australian Antarctic Division (AAD) during the southern summer to operate in water between Hobart, Tasmania, and Antarctica. The vessel serves as the main lifeline to three permanent research stations, Casey, Davis, and Mawson, on the Antarctic continent (Figure 1) and provides critical support for Australia's Southern Ocean research operation. Automated meteorological measurement systems are deployed onboard the vessel,

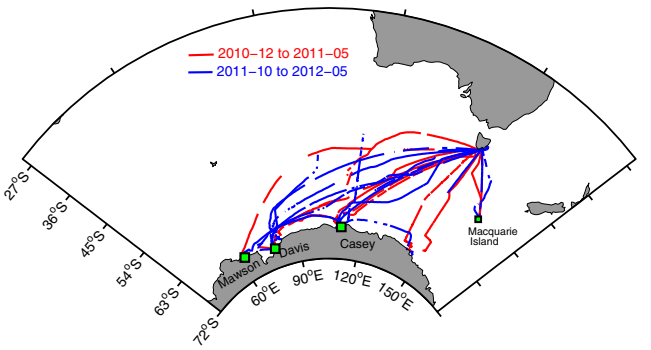

Figure 1. Ship routes operated by the icebreaker *Aurora Australis* during the southern summer between Hobart, Tasmania, and the three permanent Australian research stations, Casey, Davis, and Mawson, on the Antarctic continent. There are a total of 22 ship tracks (or 11 round trips).

providing routine observations of wind, air and sea temperature, humidity, pressure, precipitation, and downwelling long- and short-wave radiation. By using bulk flux parameterization, these measurements help determine the surface energy balance between the radiative heating and turbulent heat loss at high southern latitudes.

Two climatically important regimes are sampled as the icebreaker sails across the sub-Antarctic Southern Ocean and traverses the marginal region of the East Antarctic continent. One regime is the Antarctic Circumpolar Current (ACC) system where strong westerly winds are featured. The other is the Antarctic seasonal marginal ice zone (MIZ), i.e., the narrow transition zone that connects the ice-free sub-Antarctic with the Antarctic ice-covered regime. Observing the air-sea conditions by in situ instruments in the remote Southern Ocean has been historically challenging due to cost and logistical difficulties. The shipboard sea surface temperature (SST) and near-surface meteorological measurements acquired by the icebreaker offer a rare and valuable opportunity for gaining an in situ insight into the air-sea heat and momentum exchange in two poorly sampled yet dynamically important regimes.

The change from the ice-covered surface to open water surface creates an abrupt transition in virtually all surface characteristics [*Andreas et al*., 1984; *Bennett and Hunkins*, 1986; *Fairall and Markson*, 1987]. Strong cross-margin gradients are most evident in temperature, albedo, and roughness, all of which modify the turbulent heat and momentum exchanges as well as the radiative heat transfer over the open water surface of leads, polynyas (persistent open water), and melt ponds (in the warm season) [*McPhee et al*., 1987; *Ruffieux et al*., 1995]. In the MIZ, the sea ice acts as an insulator that keeps the water thermally inactive in the ice-covered areas. However, when leads are opened, the sensible heat flux from the open water to the air may reach several hundred watts per square meter in nonsummer seasons [*Badgley*, 1966; *Maykut*, 1978; *Andreas et al*., 1979; *McPhee et al*., 1987; *Kottmeier and Engelbart*, 1992]. Such effect is particularly pronounced during winter when temperature differences between the surface layer atmosphere and the upper ocean are 20–40°C [*Untersteiner*, 1964; *Miyake*, 1965]. The massive heat loss induces an intense cooling of the sea surface, leading to deep convective mixing and new water mass formation at some locations [*Serreze et al*., 1992; *Wadhams et al*., 2002]. The Weddell Sea is a well-known deep water formation site in the Antarctic. The region has been the focus of several field programs, including the Ice Station Weddell [*Gordon and Ice Station Weddell Group of Principal Investigators and Chief Scientists*, 1993], the Antarctic Zone Flux Experiment [*McPhee et al*., 1996], and the Ice Station Polarstern [*Hellmer et al*., 2006].

The icebreaker *Aurora Australis* crosses the sub-Antarctic Ocean and the Antarctic MIZ between 60°E and 160°E (Figure 1). This sector of the Southern Ocean has been historically undersampled. In this regard, the air-sea measurements from the vessel are valuable for filling data and knowledge gaps in regional air-sea interaction and surface energy budgets. The icebreaker measurements were made mostly during the austral spring-summer-fall months (October–April) between December 2010 and September 2012 (Figure 2). No measurements were made for the austral winter months (June–August in the sub-Antarctic and June–October in the MIZ). The MIZ in the summer months is composed of ice of different types and thicknesses, with open water in the form of leads and melt ponds [*Wadhams et al*., 1987]. There were no reports of sea-ice conditions associated with the icebreaker's measurements in the MIZ. In using the data, we assume that the icebreaker, when in the MIZ according to daily satellite measurements, navigated preferably in thin ice and open water areas between floes, and that the measurements primarily represent atmospheric conditions over the water surfaces surrounded by ice within a few kilometers.

Ship-based estimates of the surface fluxes over the Southern Indian Ocean are rare and hence, highly valuable. However, they have many uncertainties. For instance, the shipboard measurements were subject to

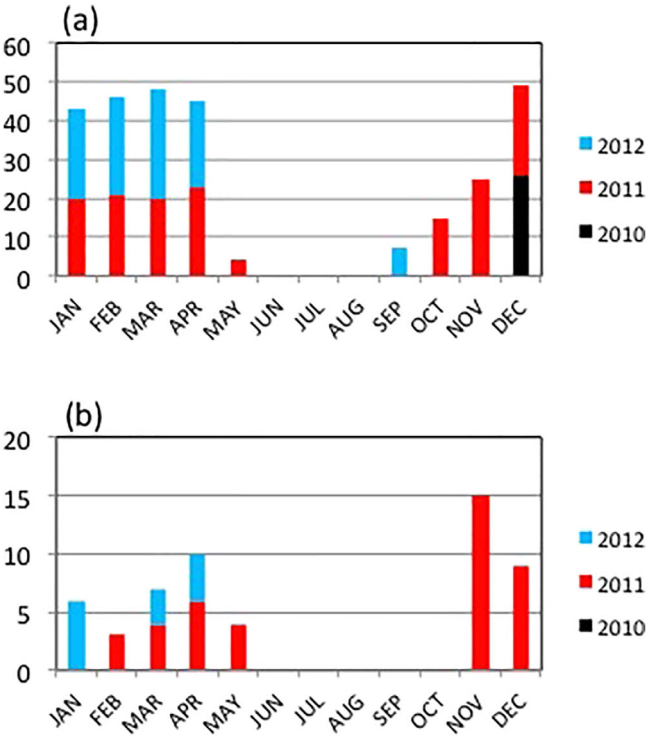

Figure 2. (a) Number of useful measurement days for each calendar month that are derived from raw data acquired along all 22 ship tracks. (b) Number of useful measurement days in the marginal ice zone.

the frequent influence of synoptic weather variability during the voyage across the ACC and into the ice margin. In addition, surface turbulent fluxes estimated from these measurements were subject to the uncertainties of the bulk flux parameterizations, which are not well tuned to MIZ surface conditions. The MIZ has different aerodynamic properties compared to the open sea because of the change of the roughness lengths for wind speed, temperature, and humidity over a surface that consists of sea ice and water [*Andreas et al.*, 2010]. Parameterizing the roughness lengths in the MIZ remains a challenging issue, though many efforts have been made. A unified form that is applicable from the open sea to the MIZ on the global scale is not yet available, indicating that the surface energy budget of the MIZ derived from shipboard air-sea measurements would be affected by the algorithm-induced uncertainty. Nevertheless, the value of the measurements is clear, and we assume that physical variations are greater than the errors introduced by using parameterizations not optimized for the MIZ conditions. The ship recorded air-sea conditions of the two climatically important regimes in this logistically difficult part of the world provide a unique opportunity to gain insights into the interplay of the atmosphere with the ocean when it exhibits different surface roughness characteristics.

The main objective of the study is thus clear: to understand the air-sea conditions measured by the icebreaker, to understand the air-sea energy budget determined from these measurements, and to characterize and compare air-sea interaction over the sub-Antarctic Southern Ocean and the MIZ. The presentation is organized as follows. Section 2 provides a description of the ship measurements and processing, the definition of the MIZ, and the computation of the ship-based air-sea fluxes. Section 3 presents the analysis results. Summary and conclusions are included in section 4.

Table 1. List of the Start and End Dates, Duration, and the Number of Useful Measurement Days for the 11 Round-Trip Cruises Used in the Study

Cruises	Start Date	End Date	Duration	Obs. Days
1	2 Dec 2010	31 Dec 2010	30	30
2	4 Jan 2011	6 Feb 2011	34	30
3	7 Feb 2011	17 Mar 2011	39	36
4	18 Mar 2011	18 Apr 2011	32	32
5	20 Apr 2011	5 May 2011	16	16
6	14 Oct 2011	30 Nov 2011	48	47
7	2 Dec 2011	31 Dec 2011	30	29
8	2 Jan 2012	15 Mar 2012	74	70
9	17 Mar 2012	14 Apr 2012	29	29
10	15 Apr 2012	1 May 2012	17	17
11	17 Sep 2012	23 Sep 2012	7	7

2. Ship-Based Measurements and Air-Sea Fluxes

2.1. Shipboard Measurements

The icebreaker *Aurora Australis* is instrumented to collect underway meteorological and oceanographic observations including wind speed and direction, air temperature (T_a), relative humidity (RH), air pressure, SST, downwelling long-wave (LW), and short-wave (SW) radiation (Table 1). The vessel typically starts from Hobart, Tasmania, traversing the sub-Antarctic Southern Ocean and the MIZ before reaching the three permanent research

stations (Casey, Davis, and Mawson) on the Antarctic continent, and then returning to Hobart (Figure 1). The start date, end date, and the duration of each round-trip operation are listed in Table 1. The ship records between December 2010 and May 2012 are used here, which were obtained from a total of 11 round-trip ship operations (or 22 ship tracks between Hobart and the Antarctic continent).

During each voyage, data streams are fed into the existing ship data management system, broadcast via satellite back to Australia every 30 min. Air-sea fluxes are calculated using the bulk flux parameterization of COARE 3.0 [*Fairall et al*., 2003]. Two daily files are delivered on a near real-time basis, the 1 min averages of surface meteorological observations and the 5 min averages of the calculated bulk fluxes. The data quality control (QC) and the subsequent generation of observation and flux data files are processed at the Australia Bureau of Meteorology as part of the Australian Integrated Marine Observing System (IMOS) [*Meyers*, 2008; *Hill*, 2010]. Since there are dual sensors for RH, T_a, SW, and LW on port and starboard and one wind sensor on the main mast, the QC procedures identify suspect observations and select observations to use in the bulk flux calculations. Specifically, RH and T_a are flagged if they exceed physical limits. The computation of the 5 min bulk fluxes uses the wind from forward of the beam and the upwind RH and T_a. The 1 min SW measurement is the highest value of the sensor pair (the lower value is more likely to be shaded by the superstructure), while the 1 min LW measurement is based on the mean of the sensor pair. These QC steps are designed to minimize the impact of the ship on the surface meteorological measurements and fluxes. Testing of the QC procedures was performed for the IMOS research vessel Southern Surveyor using a moored buoy at the Southern Ocean Flux Station (142.0°E, 46.8°S), where the ship and buoy were colocated for 23 h (see *Schulz et al*. [2012] for detailed testing results).

2.2. Air-Sea Turbulent and Radiative Fluxes Processed at Sea

Air-sea fluxes of momentum (τ, also called the surface stress) and sensible (*SH*) and latent (*LH*) heat are processed at sea using shipboard measurements (Table 1) as input to the bulk flux parameterization of COARE 3.0 [*Fairall et al*., 2003]. The main equations of the bulk flux algorithms take the forms:

$$\tau = \rho c_d W^2 \tag{1}$$

$$\mathrm{LH} = \rho L_e c_e W\ (q_s - q_a(rh)) \tag{2}$$

$$\mathrm{SH} = \rho c_p c_h W\ (T_s - T_a) \tag{3}$$

where ρ is the density of air, W the wind speed, L_e the latent heat of evaporation, c_p the specific heat capacity of air at constant pressure, and c_d, c_e, and c_h the turbulent exchange coefficients for momentum (or the drag coefficient), latent heat, and sensible heat, respectively. The ship observed quantities are the wind speed, *W*, air temperature, T_a, relative humidity, rh, and SST T_s. The specific humidity at the sea surface, q_s, is a function of T_s.

The net short-wave radiation, SW, is calculated as

$$\mathrm{SW} = \mathrm{SW}\downarrow(1-\alpha) \tag{4}$$

where SW$\downarrow$ is the measured incoming solar radiation, and α is surface albedo and set to the standard COARE3.0 constant value of 0.055.

The net long-wave radiation, LW, is computed from the following algorithm

$$\mathrm{LW} = (\varepsilon\sigma T_s^4 + \alpha_L \mathrm{LW}\downarrow) - \mathrm{LW}\downarrow \tag{5}$$

where LW is defined positive upward that corresponds to a surface heat loss, LW$\downarrow$ is the measured incoming long-wave radiation, and the term inside the bracket on the right-hand side is the estimated outgoing long-wave, with σ being the Stefan-Boltzmann constant (5.67×10^{-8} W m^{-2} K^{-4}), ε the effective emissivity of sea surface and set to be constant value of 0.97. α_L is the surface long-wave albedo and often replaced by $1-\varepsilon$ in practice. T_s is the absolute surface temperature expressed in Kelvins (K).

3. Reprocessing Shipboard Measurements and COARE-Based Air-Sea Fluxes

Although the data package provided by the icebreaker *Aurora Australis* includes both shipboard measurements of surface variables (Table 2) and COARE-based estimates of air-sea turbulent and net radiative fluxes,

Table 2. List of the Shipboard Measurements and the Height of Measurements

Observation	Instrument	Location	Height Above Water (m)
Wind speed and direction	RM Young 05106	Main Mast	31
Air temperature	2 × Vaisala HMT33	Main Mast, cross-tree, port and starboard	20
Relative humidity	2 × Vaisala HMT33	Main Mast, cross-tree, port and starboard	20
Air pressure	Vaisala PTB220	Bridge	16
Water temperature	Seabird SBE 38	Water intake	−5
Long-wave radiation	2 × Eppley PIR	Above bridge, port and starboard	18.5
Short-wave radiation	Middleton EQ08 Solar Pyranometer	Above bridge, port and starboard	18.5

reprocessing the entire data package is highly necessary. Three issues need to be resolved before ship observations can be better represented: (i) irregularly spaced measurement time series with numerous data gaps, (ii) the lack of observations of sea-ice conditions along the ship track, and (iii) the lack of representation of the MIZ surface conditions in the COARE bulk flux algorithm.

3.1. Defining the MIZ

Sea ice conditions were not included in ship data reports. We resort to daily sea-ice concentration (SIC) derived from the Special Sensor Microwave Imager (SSM/I) by the National Sea Ice Data Center (NSIDC) to depict the seasonal extension of the MIZ in the region tracked by the icebreaker. It should be noted that the SSM/I-derived SIC is an averaged over an area of approximately 25 × 25 km^2 (∼625 km^2), while ship observations are point values. Hence, the satellite area-averaged SIC represents only the general sea-ice condition within an area of 25 × 25 km^2 around the icebreaker. The actual sea-ice state along the ship's track line may have been significantly different.

Following *Strong and Rigor* [2013], we define the MIZ as the region that has the SIC greater than 15% (the sparse ice) but less than 85% (the pack ice).

3.2. Treatment of Irregularly Spaced Time Series With Data Gaps

Despite the high-frequency measurements, there were days that onboard measurements were only available for limited and irregular hours. For those days, the measurements were not able to document a full diurnal cycle, in particular for short-wave radiation, and need to be excluded to minimize the effects of aliasing associated with uneven sampling. To do so, we reprocessed the 1 min time series of surface meteorology and 5 min time series of air-sea fluxes by averaging them on an hourly basis. If the diurnal peak values were missing and the diurnal cycle could not be fully depicted, the data for that particular day were not included. Daily-mean time series along ship tracks were constructed. The number of useful measurement days for each round-trip cruise is summarized in Table 1.

Ship measurements are point measurements; they tended to be noisy and influenced by synoptic and local variability. To better represent the ship-sampled mean conditions, the measurements were binned onto 0.25° grids, grouped onto calendar months according to the date of the measurements, and then averaged zonally over all ship tracks for each month (Figure 2a). The 22 ship tracks produced more than 40 days of usable measurements for austral summer and early fall from December to April, about 15–25 days for each spring month from October to November, and less than 10 days of measurements for late fall and early spring (May, September). No measurements were made for the winter months (June–August). The data were also subgrouped for the Antarctic MIZ (Figure 2b) for the two austral summer seasons, October 2010 to May 2011 and October 2011 to May 2012. The two periods were averaged to produce a mean 2 year climatology for the following analysis.

Using the satellite SIC information, the mean monthly variations of the MIZ during the 7 month period are depicted (Figure 3a). The 7 month maximum meridional extension of the MIZ (i.e., the northernmost edge of 15% SIC) is marked by a blue line, and the number within the line denotes the number of months that the grid location has a SIC below 15% and can be regarded as open water location. The Antarctic ice in the MIZ is mostly seasonal ice [*Allison*, 1989]. During the 7 month period, the outer edge of the MIZ retreated from the seasonal maximum extension at roughly 58°S all the way to the coast off the Antarctic continent. We refer to the region encircled by the northernmost edge of the 15% SIC (i.e., the blue line) as the seasonal MIZ.

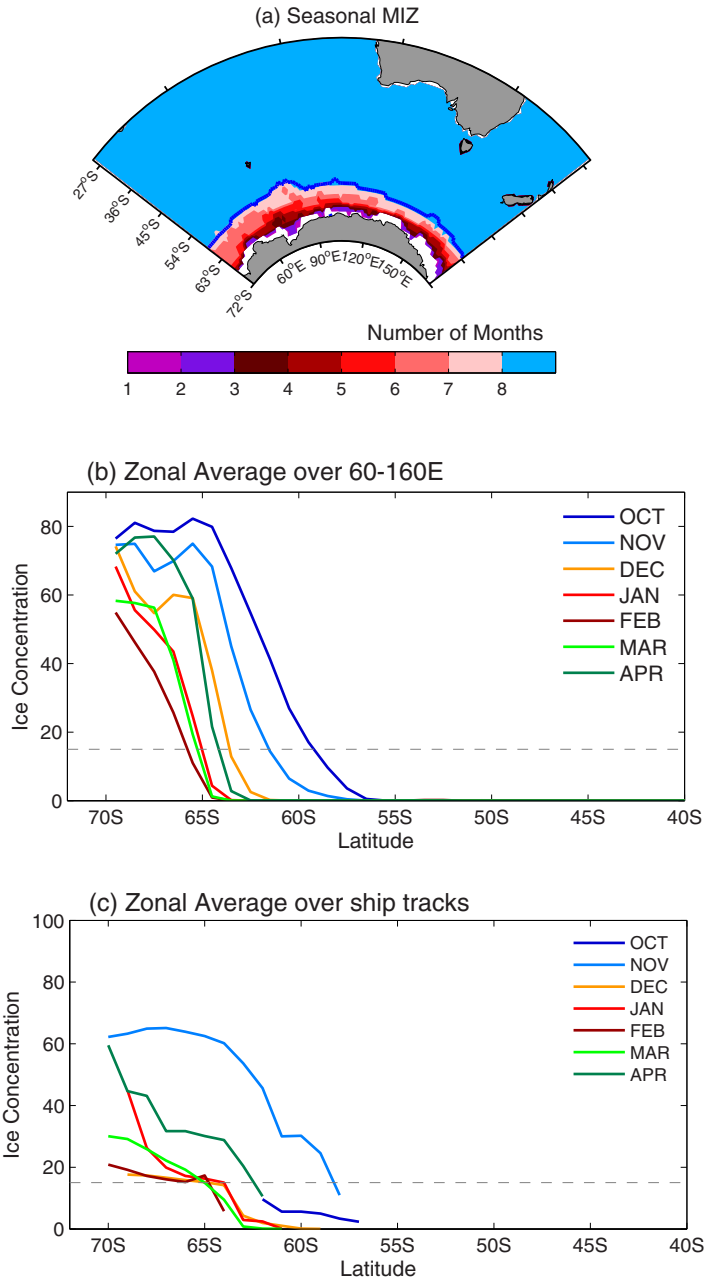

Figure 3. (a) Mean monthly variations of the edge of the 15% SIC from October to April constructed from NSIDC for the 2010–2012 ship measurement period. The thick blue line denotes the position of the seasonal MIZ, and the number within the MIZ denotes the number of months that meets the open-water condition (i.e., SIC $<$ 15%). (b) Zonal average of monthly mean SIC over the region between 60°E and 160°E, and (c) zonal average of the SIC that corresponds to each ship observation over each calendar month. In Figures 3b and 3c, the dashed line denotes the 15% SIC level, which is defined as the seaward edge of the marginal ice zone.

To characterize the seasonal progression of the MIZ in the region tracked by the icebreaker, two sets of plots were made. One plot (Figure 3b) was based on the monthly SIC zonally averaged over the area of 60°E–160°E that encompassed all 22 ship tracks (Figure 1). It shows that the 15% SIC edge was northernmost in October at ~58°S, and southernmost in February at ~66°S. The other plot (Figure 3c) was based on the zonal averages of the SIC that corresponds to each ship observation. The plot shows a pattern similar to that of the regional average (Figure 3b), albeit with a much reduced SIC (Figure 3c). The reduced SIC may well be an indication that the icebreaker navigated preferably on the thin ice and open water areas in the sea-ice margin. Hence, the ship measurements may represent the atmospheric conditions more over the water surface than over the ice surface. A clear distinction of the two surfaces is necessary. The change from aerodynamically smooth to aerodynamically rough surfaces causes strong cross-margin gradients in temperature, albedo, and roughness, all of which affect the turbulent heat and momentum exchanges as well as the radiative heat transfer in the MIZ.

3.3. Resolving Air-Sea Fluxes in the MIZ

The COARE bulk flux algorithm [*Fairall et al.*, 2003], which was implemented by the icebreaker to process ship-based air-sea heat fluxes at sea, is not tuned for the applications in the MIZ. The surface properties in the MIZ are widely variable. In addition to the change of aerodynamic roughness, the large $T_s - T_a$ is a destabilizing factor for the near-surface flow. *Andreas and Murphy* [1986] showed that the instability promotes heat transfer by free convection until turbulent mixing erodes the vertical temperature profiles and resets the equilibrium. *Andreas* [1987] proposed a turbulent surface-renewal model to predict neutral-stability values of c_e and c_h as functions of W and a surface roughness parameter. *Andreas et al.* [2010] developed a unified bulk flux parameterization for turbulent fluxes over summer sea ice and any marginal ice zone, using data collected

at multiple sites during the year-long experiment of the Surface Heat Budget of the Arctic Ocean (SHEBA). Since the scope and complexity of the SHEBA algorithm are structured in a way similar to those of the COARE algorithm, merging the two algorithms stands as a natural choice.

The essence of the SHEBA bulk flux algorithm is the determination of c_d, c_e and c_h, the turbulent transfer coefficients for momentum (or the drag coefficient), latent and sensible heat (equations (1–3)), for the mixed ice and water conditions in the MIZ. These transfer coefficients are commonly parameterized on the basis of the Monin-Obukhov similarity theory. It is worth noting, however, the difference between the SHEBA and COARE 3.0 algorithms in terms of parameterizing surface roughness. In the COARE 3.0 scheme, the surface roughness is dependent of wave height and wave period for well-developed seas over the open ocean, and this dependence is present through the Charnock relation using either observed wave characteristics or assumed open-ocean waves. The SHEBA algorithm, on the other hand, does not include the effect of wave-induced roughness. Furthermore, wave characteristics within the MIZ certainly cannot be represented by open-ocean waves.

Full details of how the SHEBA algorithm adjusts the parameterization of roughness lengths in sea-ice conditions are provided in *Andreas et al*. [2010], from which two distinctive features is worth mentioning here. One is the inclusion of form drag in parameterizing c_d. Form drag is a unique aerodynamic feature in the MIZ, where the open water in leads and melt ponds creates vertical sea-ice faces that the wind can push against, enhancing momentum transfer through form drag (i.e., pressure forces) [*Arya*, 1973, 1975; *Rao et al*., 1974; *Andreas et al*., 1984]. The other feature is the use of a mosaic method [*Vihma*, 1995] to estimate turbulent heat fluxes. The surface of the MIZ is a patchwork of sea ice, melt ponds, and leads. The mosaic-based method computes the latent and sensible heat fluxes as weighted averages of the fluxes from heterogeneous surfaces. As a result, the algorithm has one extra term, namely, the latent heat of sublimation over ice, in addition to the latent heat of vaporization over the open water (leads and ponds). In the algorithm, the weighted averages are based on the SIC that is provided as an input.

Short-wave incoming radiation, SW↓, was measured by the icebreaker, but surface albedo was not measured. The latter is required for computing the total net downward solar radiation, SW (equation (4)). Surface albedo varies greatly with ice types of varying thickness and snow cover [*Katsaros, et al.* 1985; *Sedlar, et al*. 2011]. *Maykut and Perovich* [1987] suggested an average value of the lead albedo about 0.1 based on the direct measurements made during the summer 1984 Marginal Ice Zone Experiment (MIZEX) in the Fram Strait. *Francis et al*. [1991] proposed that the albedo in the MIZ should be a weighted average of the ice, water, and melt pond albedos and the SIC. *Allison et al*. [1993] indicated that Antarctic sea ice is mostly young or first-year ice because most of the ice melts during the following summer after it forms. Albedo is low over new ice, but increases gradually as the ice thickens. *Allison et al*. [1993] computed the area-averaged albedos in the MIZ using representative all-wave albedos derived from the spectral albedo measurements and the ice type observations. *Brandt et al*. [2005] refined the approach and proposed the following algorithm for obtaining the area-average albedo, α, in the MIZ:

$$\alpha = \alpha_i c_i + \alpha_w (1 - c_i) \tag{6}$$

where α_i is the ice-only albedo, α_w the albedo of open water that is set at 0.055 [*Fairall et al*., 1996], and c_i the sea-ice concentration. In this study, c_i is extracted from SSM/I along each ship track (Figure 3). The values of α_i are a function of latitude and season that are produced by *Brandt et al*. [2005] for all-wave, cloudy-sky incident irradiance using albedo measurements from three ship-based field experiments in the Antarctic sea ice zone.

In computing LW (equation (5)), the incoming component, LW↓, was measured by ship. The outgoing component is parameterized and includes two processes, the emitted LW that is approximated by the black body radiation and the reflection of LW↓ that depends on the long-wave albedo, α_L (or long-wave reflectivity). Little is known about the value of α_L, although in general the long-wave reflectance of the water surface is less than 5% [*Clark et al*., 1974]. It has become a common practice to relate α_L to $1 - \varepsilon$ and rewrite equation (5) as follows:

$$\mathrm{LW} = (\varepsilon\sigma T_s^4 + (1-\varepsilon)\ \mathrm{LW}\downarrow) - \mathrm{LW}\downarrow = \varepsilon(\sigma T_s^4 - \mathrm{LW}\downarrow) \tag{7}$$

where a constant ε of 0.97 is often used [*Fairall et al*., 1996]. The effect of sea ice on ε in the MIZ is assumed small, because the surface temperature of sea ice and water do not vary much around the freezing point,

particularly during the summer season [*Kergomard et al.*, 1993]. In equation (7), T_s is a skin temperature and is not equal to the bulk SST measured by ship. The correction of cool skin effects in the COARE Algorithm [*Fairall et al.*, 2003] was applied.

4. Analysis

4.1. Winds

Among the four measured basic variables, winds are the most variable in time and space. Monthly mean latitudinal variations of ship-measured W are constructed (Figure 4a). The latitude of the 15% SIC (i.e., the outer edge of the MIZ) for each month is marked on the *x* axis of the top plot using the designated color code. The northernmost extent of the edge of the15% SIC occurred in October at ~58°S, and the position is taken as the boundary of the seasonal MIZ (marked by the dashed line). Stronger winds are observed in two places. One is the ACC area between 58°S and 52°S, where monthly mean W ranges between 10 and 18 m s^{-1} during the 7 months. The other place is the inner edge of the seasonal MIZ (i.e., the area off the coast of the Antarctica), where monthly mean W reached 8–10 m s^{-1} in February–March and exceeded 15 m s^{-1} in November. High winds are a trademark of the ACC region, and the observations are as expected. The highly interesting feature revealed by the ship measurements is the pattern of the wind changes within the MIZ. Winds were weak within the MIZ near the outer edge (62°S–60°S). Once the air moved out to the open sea, it accelerated equatorward. Observations indicate that the winds over the ice margins were predominantly southerly during the seven months (not shown). Therefore, the off-ice airflow experienced a downstream convergence within the MIZ followed by a divergence when moving out to the open ocean.

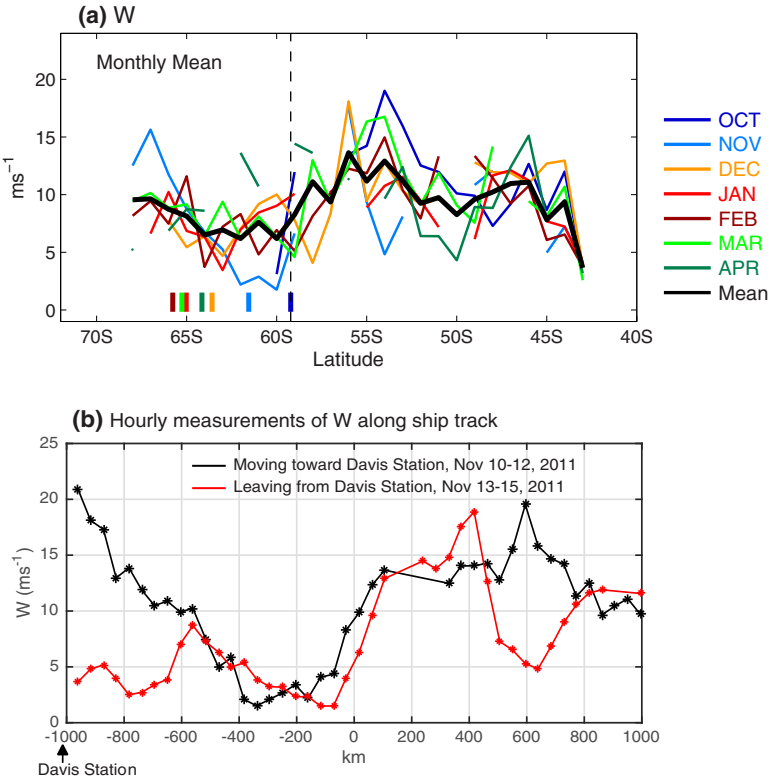

Figure 4. (a) Monthly mean variations of wind speed zonally averaged over the areas tracked by the icebreaker between Hobart, Tasmania (43°S) and the Antarctic continent. The thick black line represents the 7 month mean. The latitude of the monthly MIZ is marked on the *x* axis using the matching color code, and the seasonal MIZ is denoted by the vertical black dash line. (b) Hourly mean shipboard wind speed measurements along the track toward the Davis Station during 10–12 November 2011 (black line) and away from the station during 13–15 November 2011 (red line), with star (*) marked the location of hourly measurements. Location of the MIZ (at 59.35° latitude) is defined as 0 km (reference position), and the distance is labeled negative when moving poleward from the reference position and positive when moving seaward away from the MIZ.

The band structures of winds in the ice margins have been studied extensively [*Guest et al*., 1995], as winds are the ultimate force for sea ice drift [*McPhee et al*., 1987]. The alternating convergence and divergence in the MIZ were first reported on two cruises in the Bering Sea [*Muench and Charnell*, 1977; *Bauer and Martin*, 1980]. Within the convergence, rafting occurs which further roughens the surface; meanwhile the downwind divergence tends to accelerate the ice seaward, contributing to a diffuse ice edge. These mesoscale bands of winds are thought to be responsible for the observed mesoscale banding of ice concentrations in the MIZ [e.g., *Muench and Charnell*, 1977; *Hakkinen*, 1986]. *Overland et al*. [1983] successfully simulated the phenomenon using a one-layer model of the atmospheric boundary layer over the MIZ. They suggested that the band structure of winds was a result of the effects of the changing surface roughness on the turbulent momentum flux [*Overland*, 1985; *Anderson*, 1987; *Fairall and Markson*, 1987; *Guest and Davidson*, 1987]. For off-ice flow, the increased physical roughness from the pack ice to rough ice to open water leads to an increase of aerodynamic roughness. *Andreas et al*. [2010] and *Elvidge et al*. [2016] showed that the parameterization of c_d in the polar MIZs needs to account for two effects. One is the skin drag of the open water surface and the other is the form drag at the vertical ice faces created by leads and melt ponds [*Arya*, 1973, 1975]. The effects of the two drags results in a nonlinear dependence of c_d on the SIC [e.g., *Andreas et al*., 1984; *Overland*, 1985]. There is a general consensus that c_d peaks when the SIC is in the range 50–60% and decreases for lower and higher SIC [*Andreas et al*., 1984; *Guest and Davidson*, 1987; *Anderson*, 1987; *Birnbaum and Lüpkes*, 2002]. It is observed from Figure 3c that the SIC was highest in November, with 50–65% SIC dominating the section between 70°S and 63°S. The wind speed was also strongest in November (Figure 4a). For other months, the SIC was way below 50% except for April, during which the SIC spiked to 50% and greater near the coast of Antarctica. Overall, a smaller amount of sea ice corresponds to a weaker wind speed.

The observed deceleration of the airflow by increased surface roughness appears to support the previous findings that surface roughness affects not only c_d but also W [*Bauer and Martin*, 1980; *Martin et al*., 1983; *Andreas et al*., 1984; *Smith and MacPherson*, 1996]. While the cause of the former is attributed to the aerodynamic response [*Andreas et al*., 2010], the mechanism of the latter is proposed to be the dynamical adjustment of ABL to the spatially varying surface drag [*Rao et al*., 1974]. *Kantha and Mellor* [1989] used a two-dimensional multilevel model and obtained similar results to those of *Overland et al*. [1983]. They both showed that the off-ice deceleration of the airflow is a response of the ABL to the locally rough sea. The increased surface drag increases the momentum flux, which in turn thickens the ABL and weakens W. The thickness of the ABL is further boosted by the influx of large turbulent heat over the open water leads and melt ponds, leading to a weak W near the outer edge of the MIZ. Once out of the MIZ, the ABL thickness reduces as the surface drag reduces, but the sea surface temperature increases. The warmer sea surface destabilizes the ABL, mixing down the momentum from higher levels, and causing the near-surface airflow to accelerate. *Overland et al*. [1983] and *Kantha and Mellor* [1989] showed that there was an increase of wind speed by about 10% from the rough ice edge to open water. They suggested also that the intensity of the ice edge winds might be a function of the near-surface atmospheric stability, stronger in winter and weaker in summer.

For the 7 months of this study, winds in the MIZ were strongest in November (Figure 4a). To take a close look at the change of wind in the MIZ, we followed the ship track in November 2011 that sailed poleward across the MIZ on 10 November to arrive at Davis Station on 12 November, and then left the station the following day to sail across the MIZ on 15 November on the way back to Hobart. The 15% SIC, which was located at 59.35° latitude, is set as 0 km, the reference position. The ship measured winds and measurement distances relative to the reference position were plotted on hourly basis (Figure 4b). The distance is labeled negative when the icebreaker moving toward the Davis Station from the reference position, and positive when moving seaward away from the reference position. The total width of the MIZ was ~1000 km and winds were predominantly southerly in the MIZ. It can be seen that, within the vicinity of the MIZ between −600 and 300 km, the pattern of the wind speed changes observed by the en route trip agrees well with that observed by the returning trip. Both registered the deceleration (convergence) and the acceleration (divergence) at the ice edge. This pattern of the wind changes across the MIZ appears to be consistent with the model simulation of *Overland et al*. [1983] and *Kantha and Mellor* [1989], albeit the magnitude of the wind increase was much greater than the modeled results. Outside of the MIZ vicinity, the wind speed change pattern differs between the en route and the returning trips. For instance, near the coast of Davis

between −1000 and −600 km, the en route trip observed a sharp increase in W from 10 m s^{-1} at −600 km to 21 m s^{-1} at −1000 km, while the returning trip experienced mild winds around 3–5 m s^{-1}.

4.2. Near-Surface Thermodynamic Variables

The ship-based monthly mean latitudinal variations of the sea-air thermal variables, T_s and T_a (Figures 5a and 5b) show a strong latitudinal dependence. T_a decreases near linearly poleward while T_s also decreases but at a slower rate as it approaches the freezing point of seawater in the MIZ. Within the MIZ, T_s was mostly at −1.9°C, the freezing temperature of sea water, while T_a varied widely. T_a changed from −5°C in spring (November) to near 0°C in summer (December–January), and down to −8°C again in fall (February–April). The large fluctuations of T_a caused the sea-air temperature difference, $T_s - T_a$, to change sharply with the season (Figure 5c). $T_s - T_a$ was ∼+6°C in spring (November), down to near 0°C in summer (December–January), and up again to more than 10°C in late fall (March–April). When averaged over October–April (black line) the mean values for $T_s - T_a$ in the sub-Antarctic Southern Ocean is consistently close to zero while in the MIZ it increases from close to zero to 4–8°C at the southern boundary. The ship measurements did not include the winter season. It has been reported that sea-air temperature differences in winter could be in the range of 20–40°C [*Untersteiner*, 1964; *Miyake*, 1965; *Andreas et al.*, 1984; *Bennett and Hunkins*, 1986].

The specific humidity, q_a, shows also a decrease with increasing latitudes. q_a decreased from about 8 g/kg at 43°S to 2 g/kg at 68°S (Figure 5d), suggesting that air in the MIZ was extremely dry. The range of monthly

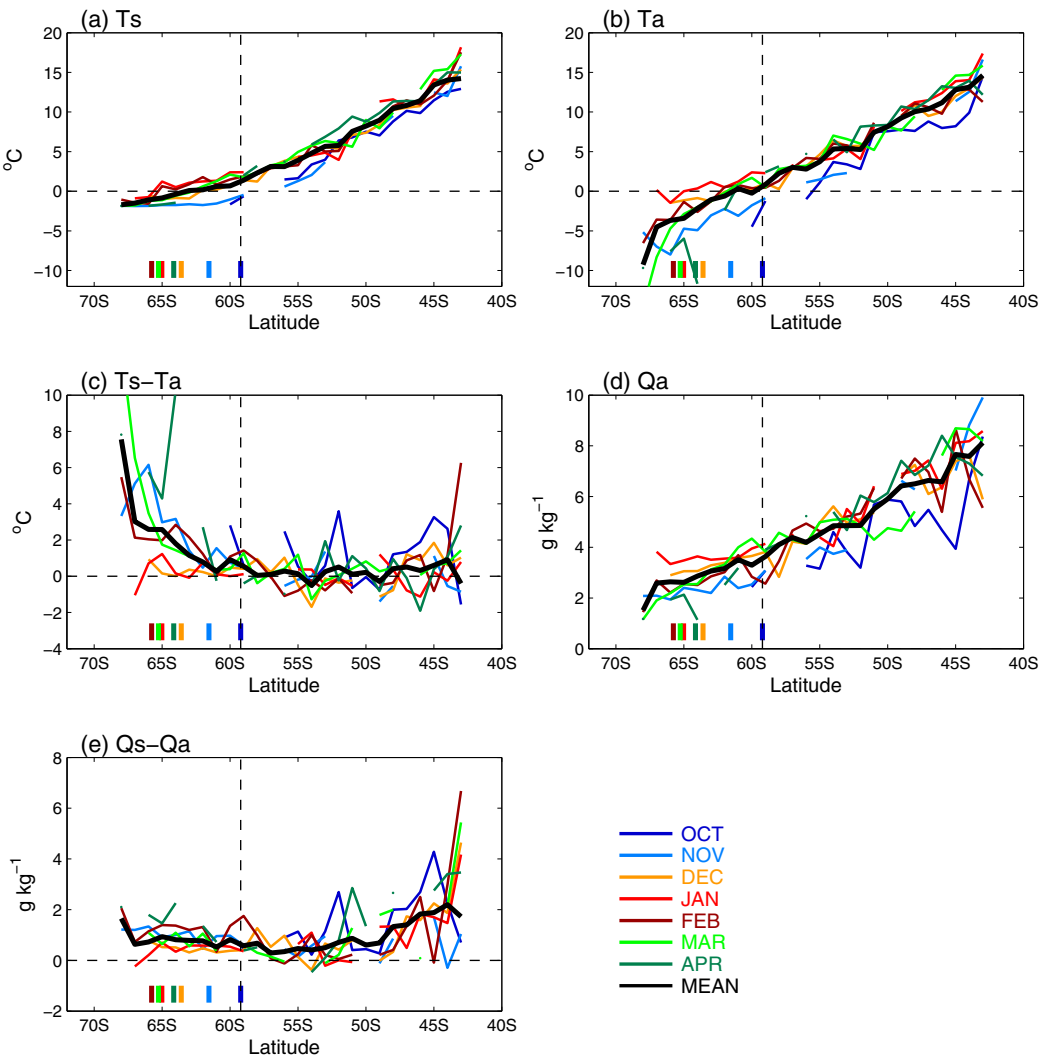

Figure 5. Same as Figure 4a but for (a) T_s, (b) T_a, (c) $T_s - T_a$, (d) q_a, and ($q_s - q_a$).

q_a variability was also relatively low over the MIZ compared to the q_a variability over the warmer sub-Antarctic. Following the Clausius-Clapeyron equation, the moisture holding capacity is low when air is cold. Hence, while q_a is small, the air is still close to saturation and relative humidity observations exceed 90% most of the time (not shown). High relative humidity is a ubiquitous phenomenon in polar regions and have been reported in previous studies [*Persson et al*., 2002; *Andreas et al*., 2002]. Two processes are thought to be responsible for the existence of high relative humidity at high latitudes [*Andreas et al*., 2002]. One is the shallow polar marine boundary layer, allowing moisture equilibrium to be established at time scales shorter than the destabilizing time scales of synoptic processes. The other is the strong evaporation by the relatively warm sea surfaces over open leads and polynyas, which generate water vapor more rapidly than the water vapor being removed. Additional process such as sublimation (i.e., the transition of moisture directly from snow and ice) in cold seasons may also be a source [*Liston and Sturm*, 2004].

The air in the MIZ was colder (Figure 5b) and drier (Figure 5d) in spring and fall than in summer. Consequently, the sea-air differences of temperature, $T_s - T_a$ (Figure 5c), and humidity, $q_s - q_a$ (Figure 5e), were both greater in the off-summer seasons. The sea-air contrasts were strongest near the coast of Antarctica and weakest in the vicinity of the seasonal ice edge. Away from the MIZ, $q_s - q_a$ increased equatorward and was most pronounced over the warmer waters near Hobart, where the higher q_a may have been due to the exponential effect of the warmer temperature on the saturation specific humidity.

4.3. Turbulent Heat Fluxes and Surface Radiation

The turbulent heat exchanges, LH and SH (Figures 6a and 6b), show a pattern of change that was governed primarily by the respective $q_s - q_a$ (Figure 5e) and $T_s - T_a$ (Figure 5c), rather than variations in W (Figure 4a). Within the MIZ, the sharp seasonal changes in $T_s - T_a$ led to a marked increase of sensible heat loss toward the South Pole in spring and fall. SH reached 100 W m^{-2} in November and February and exceeded 200 W m^{-2} in March. SH was small in December–January when the summer air temperatures were near the freezing point. Enhanced turbulent latent heat loss was also noted during the off-summer seasons, with magnitude of 80–100 W m^{-2} south of 65°S. It is apparent that SH dominated LH in the MIZ, and the dominance was particularly striking during spring and fall. Away from the MIZ, SH was small and varied around zero (i.e., heat gain and loss) while LH became more important. LH increases equatorward as $q_s - q_a$ increases (Figure 5e).

The net solar radiation, SW, varied strongly with season, highest in December–January and lowest in March–April (Figure 6c). The difference between the two seasons was about 200 W m^{-2}. SW decreases with increasing latitude. There is a clear reduction of SW in the MIZ, due primarily to the albedo effect of the sea ice (equation (6)). On average, there is ~75 W m^{-2} reduction in net solar heating from 45°S poleward to 65°S, of which 13 W m^{-2} is due to the sea-ice effect on the change of albedo in the MIZ. The net long-wave radiation, LW, was generally weak, except for the vicinity of Hobart (Figure 6d). Monthly variability of LW was also weak, showing little changes between seasons. Within the MIZ, LW increased poleward in a manner similar to LH and SH (Figures 6a and 6b). The long-wave radiative cooling was strongest in February-March-April, which was the time of the year when the SIC was minimal (Figure 3c).

Within the MIZ, LW↓ (Figure 6e) decreases with latitude at a slower rate than upwelling LW (σT_s^4), resulting in an increase of net longwave approaching the pole in all months except January (Figure 6d). The January observations are interesting but plausible. Findings of previous studies indicate that LW↓ could be either enhanced or reduced in the MIZ, depending upon the season and the complexity of the processes that are involved. *Francis and Hunter* [2006] suggested that the increase of LW↓ during spring and summer is the primary driver of subsequent sea ice reduction in the Barents and Bering Seas. *Schweiger et al*. [2008] showed that low-level clouds over marginal sea ice decrease with decreasing ice concentration in the Arctic during fall, causing a reduction of LW↓. In cold temperatures, LW↓ over the marginal sea ice is influenced by the temperature and emissivity profiles through the atmosphere and hence, highly sensitive to low-level cloud amount and cloud base temperature [*Key et al*., 1996]. As explained by *Schweiger et al*. [2008], the changes in cloud cover are caused by modifications to the temperature and humidity structure in association with sea ice variability. When the sea ice cover is low during fall, the temperature at the base of the boundary layer increases more than at the top, decreasing static stability as well as the strength of inversion that typically caps low cloud decks. Here the LW↓ measurements in the Antarctic MIZ appear to be consistent with the Arctic observations, showing that downward long-wave radiation increases in spring and summer

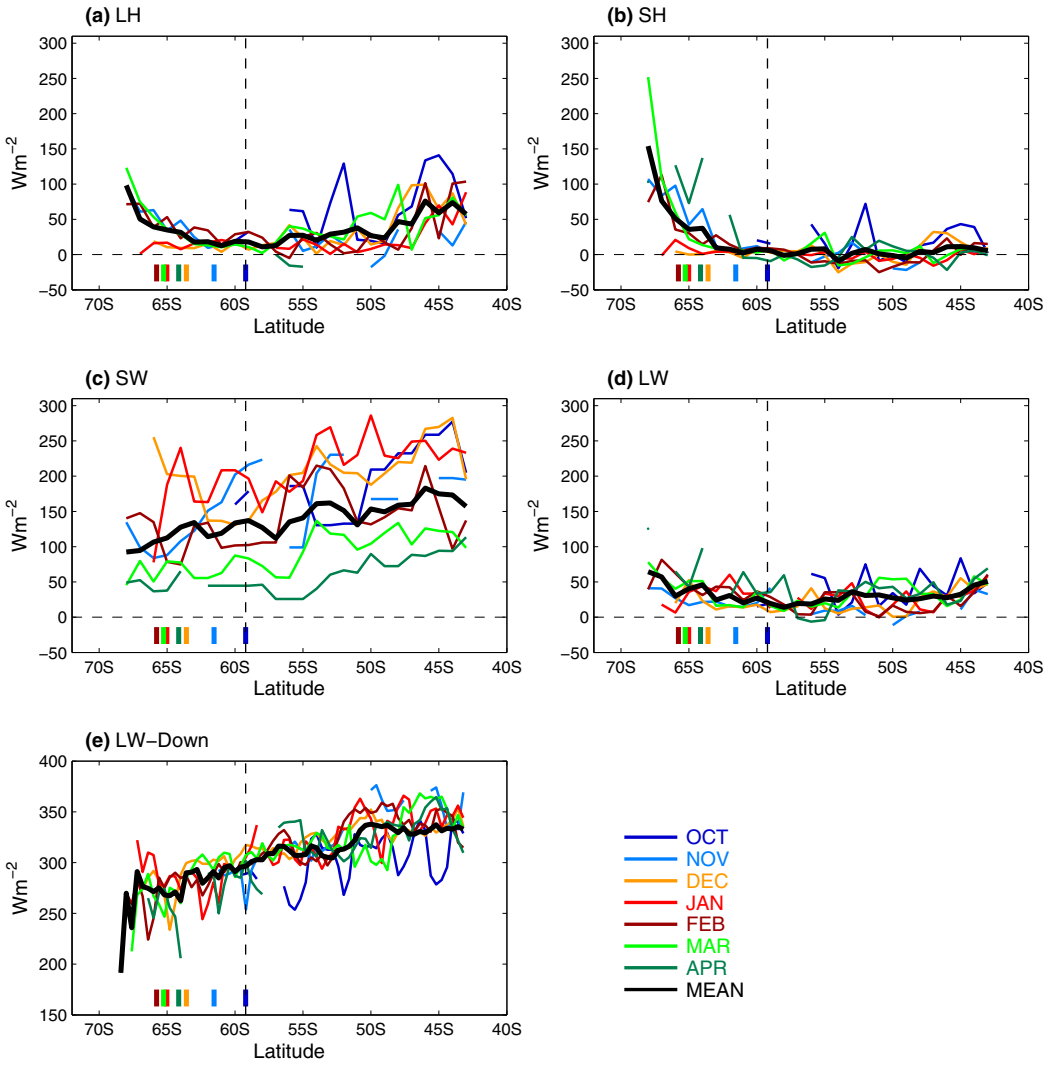

Figure 6. Same as Figure 4a but for (a) LH, (b) SH, (c) SW, (d) LW, and (e) LW downward component. Note that positive values of LH, SH, and LW correspond to a surface heat loss, whereas positive values of SW and LW downward correspond to a surface heat gain.

[*Francis and Hunter*, 2006] but decreases in fall [*Schweiger et al.*, 2008]. However, it may need to add a word of caution, as the small sample size may not be sufficient to draw firm conclusions.

4.4. Q_{net}

Month-to-month variations of the total air-sea turbulent heat fluxes, LH + SH (defined positive upward), the total surface radiation, SW − LW (defined positive downward), and the sum of all these terms, Q_{net} = SW − LW − LH − SH (defined positive downward), are shown in Figures 7a–7c. The 7 month mean is also superimposed in each plot. Over the sub-Antarctic Southern Ocean (58°S–43°S), LH+SH was generally less than 20 W m^{-2}, except for the section near Hobart (48°S–43°S) where turbulent heat loss was up to 100 W m^{-2}, due mostly to LH. Seasonal variability was rather weak away from Hobart. On the other hand, seasonal changes of SW − LW were significant. The downward radiative heating reached a maximum in January and a minimum in April, and the range of the change was more than 200 W m^{-2}. As a result, Q_{net} changed sign with season over the sub-Antarctic. The ocean surface received a net heating from the atmosphere from October to March, and lost heat to the atmosphere in April. The 7 month mean Q_{net} was positive at about 80–150 W m^{-2} in the sub-Antarctic ocean regime, except for the section near Hobart (48°S–43°S) where the radiative heat gain was more strongly offset by the turbulent heat loss.

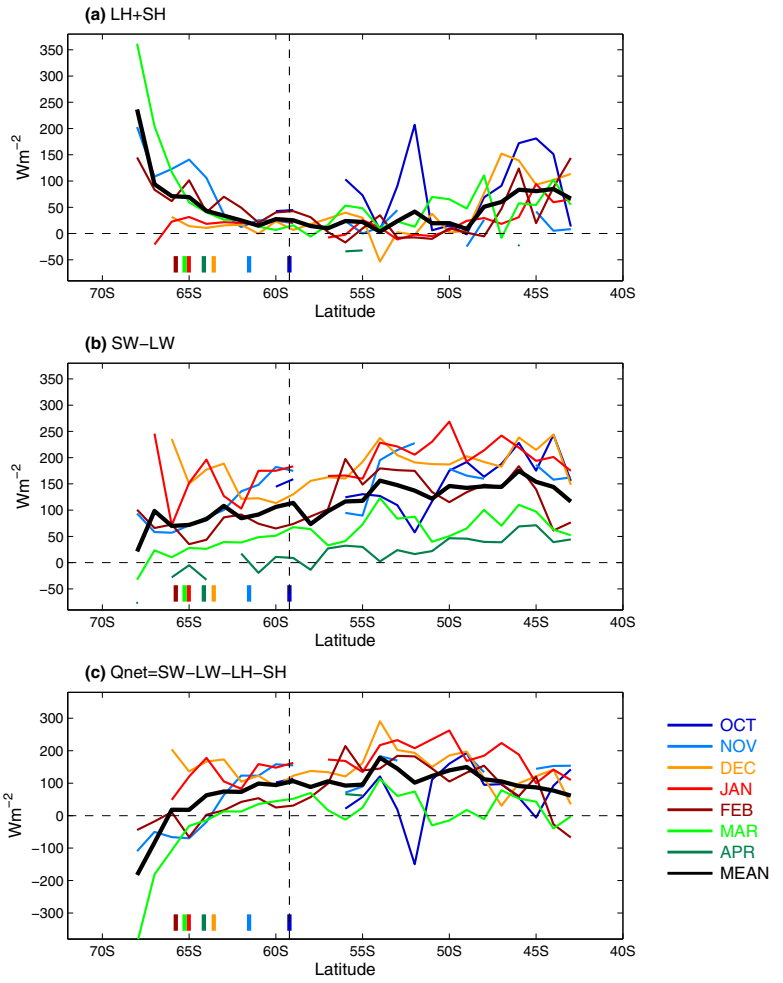

Figure 7. Same as Figure 4a but for (a) LH+SH, (b) SW-LW, and (c) Q_{net}.

Within the MIZ regime (68°W–58°S), SW-LW dominated the month to month variations of Q_{net}. Compared to the sub-Antarctic, turbulent heat loss was more pronounced. LH+SH underwent a rapid poleward increase, from about 20 W m^{-2} at the outer edge of the MIZ up to 200 W m^{-2} near the Antarctic coast. The consequent compensation on the downward radiative heating led to a sharp decline of Q_{net}. Poleward of 64°S, Q_{net} remained negative except for December–January, indicating that, near the ice edge, the ocean is a source of heating for the atmosphere for the off-summer seasons.

The differences in Q_{net} between the MIZ and the sub-Antarctic are due primarily to the differences in SW, LH, and SH between the two regimes. To see this, month-to-month variations of SW, LW, LH, SH, and Q_{net} averaged in the MIZ (68°S–58°S) are compared with those averaged in the sub-Antarctic section (58°S–43°S) (Figures 8a–8e). The comparison offers interesting insights into how the surface budget is balanced with and without the sea-ice influence. The seasonal variations of SW in the two regimes were highly similar, except for the magnitude. The net downward solar radiation in the MIZ was about 50 W m^{-2} weaker than that in the sub-Antarctic section (Figure 8a), reflecting the influence of sea-ice albedo and the reduction of solar insolation with latitude. Changes in LW across the two regimes were not as large, albeit LW loss in the MIZ tended to be slightly lower than that in the open ocean between October and November and slightly higher between January and April (Figure 8b).

Compared to SW and LW, the regime contrast in LH and SH was more pronounced (Figures 8c and 8d). LH and SH in the sub-Antarctic section featured weak seasonal variations. Over the 7 month period, SH remained near zero, while LH maintained at 40 W m^{-2} except for a slight enhancement in October–November. Quite the contrary, LH and SH in the MIZ had far more significant changes with season. LH transitioned

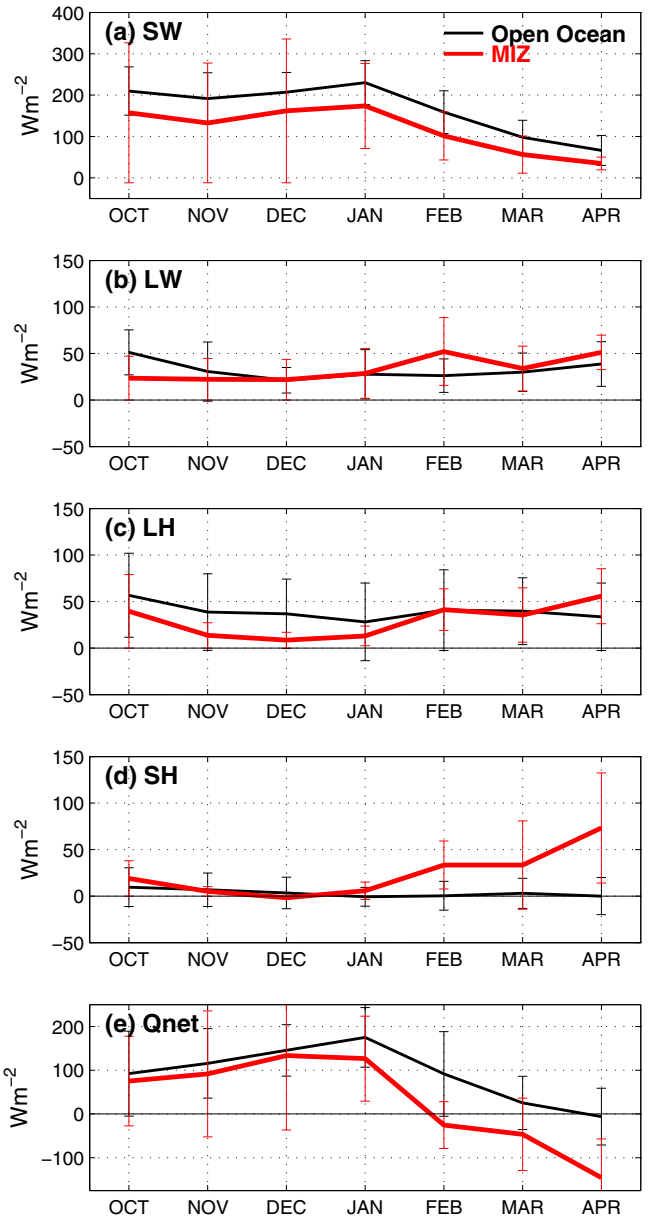

Figure 8. Comparison of monthly evolution of (a) SW, (b) LW, (c) LH, (d) SH, and (c) Q_{net} = SW – LW – LH – SH averaged in the seasonal MIZ (68°S–58°S) (red line) and the sub-Antarctic open ocean (58°S–43°S) (black line). The error bars indicate the standard deviation of the spread in the observations that were used in computing the monthly mean.

from a high of ~40 W m^{-2} in October, to a low of ~5 W m^{-2} in November and December, and to a high again at 45–50 W m^{-2} throughout February-March-April. Meanwhile, SH in the sea-ice zone had a step-like change around January: it transitioned from a near-zero state between October–January to a monotonic increase thereafter, reaching up to 70 W m^{-2} by April.

The rapid increase in SH between January and April was so pronounced that it affected the balance of the surface budget in the MIZ. During this period, SH was of a similar magnitude to LH and LW, which all together offset the net solar heating and kept the MIZ in a net heat loss regime from February to April (Figure 8e). That is, during late summer and autumn, the MIZ lost energy to the atmosphere equally from LW, SH, and LH. This is a sharp comparison to the role that SH had over the sub-Antarctic section, where SH was around zero throughout the 7 month period and its contribution to Q_{net} was negligible compared to LH and LW. However, since the seasonal variations in LH and LW were weak, the seasonal change in Q_{net} over the sub-Antarctic section was dictated primarily by the change of SW. The sub-Antarctic section remained in a net heat gain regime until April.

Standard deviation (STD) of the spread in the observations is provided as a measure of uncertainty. However, the STD spread is not entirely an uncertainty, as it can be induced by synoptic weather variability and/or interannual variability as well as by the lack of sufficient data samples. The MIZ is narrow (~1000 km) and dictated by synoptic variability. The ship measurements are, however, highly limited (Figure 2b). The number of useful measurements ranges from 3 days to 15 days for the 7 months in study—one certainly does not expect that a monthly mean can be fully represented by this limited number of measurement days. It can be seen that the STD spread is usually larger for the flux components in the MIZ than for the sub-Antarctic regime, which affects the confidence of the surface budget estimates in the MIZ.

4.5. Surface Energy Budget in the MIZ and Sub-Antarctic

The surface energy budgets averaged for the 7 months over the spring-summer-fall seasons are shown for the MIZ (68°S–58°S) and the sub-Antarctic (58°S–43°S), respectively (Figures 9a and 9b). Overall, there was a net heat gain in both regimes during the seven nonwinter months in study, with the net downward SW being the dominant component. In the MIZ, the mean SW of 117 ± 69 W m^{-2} was balanced by the net LW

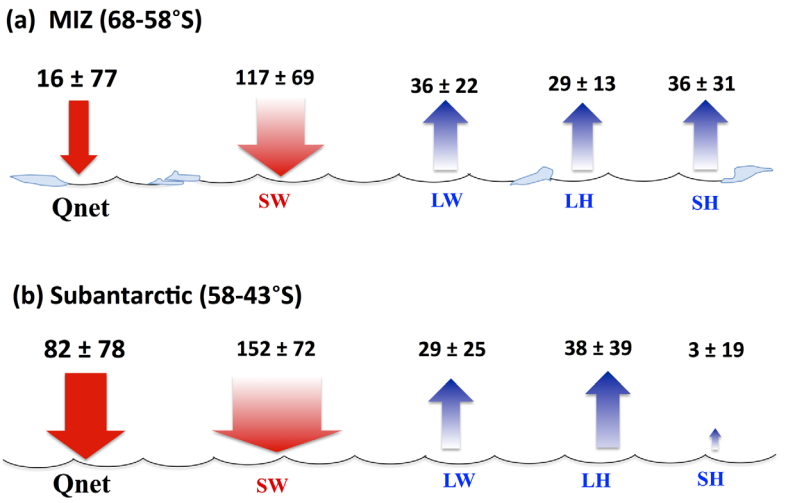

Figure 9. The energy budget (a) in the seasonal MIZ (68°S–58°S) and (b) over the sub-Antarctic open ocean (58°S–43°S). The values are averaged over the period of October–April. Uncertainty estimates represent the standard deviation of the spread in the observations that were used in computing the mean.

cooling of 36 ± 22 W m^{-2}, latent heat loss of 29 ± 13 W m^{-2}, and sensible heat loss of 36 ± 31 W m^{-2}, leading to a net heat gain of 16 ± 77 W m^{-2}. By comparison, the sub-Antarctic budget was 82 ± 78 W m^{-2}, resulting from the balance between net SW heating of 152 ± 72 W m^{-2} and cooling by LW of 29 ± 25 W m^{-2}, LH of 38 ± 39 W m^{-2}, and SH of 3 ± 19 W m^{-2}.

The net heat gain in the sub-Antarctic was 82 ± 78 W m^{-2}, which was more than 60 W m^{-2} higher than that in the MIZ. The difference was attributed primarily to the differences in SW, LH, and SH between the two regimes, as LW was less regime dependence. SW, LH and SH are directly impacted by the sea-ice-induced changes in surface albedo, roughness, and air temperature. The net radiative heating in the MIZ was about 30 W m^{-2} less compared to the sub-Antarctic ocean, and the total turbulent heat loss by LH+SH was about 30 W m^{-2} more. The two effects led to the Q_{net} in the MIZ that was 60 W m^{-2} lower than that over the sub-Antarctic water. The contribution of SH to the MIZ surface heat budget is particularly noted, as it played an equally important role as LH and LW in balancing out the net solar heating in the MIZ.

Standard deviation (STD) of the spread in the observations is considerably large, particularly in the MIZ. As pointed out in above section, the STD spread is not entirely an uncertainty, as it can be induced by synoptic weather variability and/or interannual variability as well as by the lack of sufficient data samples. For SH in the MIZ, the STD spread has the same magnitude as the mean, while for Q_{net}, the STD spread is about 3.5 times larger than the mean. The sample size in the MIZ may not be sufficient to produce acceptable statistically significant results.

5. Summary

This study analyzed shipboard air-sea measurements acquired by the icebreaker *Aurora Australis* during its summer operation in December 2010 to May 2012. The icebreaker traversed the water between Hobart, Tasmania and the Antarctic continent, measuring air and sea temperatures, near-surface humidity, wind speed, downward short-wave and long-wave radiation during the voyage. Mean conditions over the seven nonwinter months (October–April) were compiled from a total of 22 ship tracks. These shipboard measurements offer a rare and valuable opportunity for gaining an in situ insight into the air-sea heat and momentum exchange in two dynamically important, yet poorly sampled, regimes: the sub-Antarctic Southern Ocean (58°S–43°S) and the Antarctic MIZ (68°S–58°S) in the Indian Ocean sector. The MIZ is determined by the 15% sea-ice concentration provided by NSIDC, since there were no sea-ice reports from the icebreaker. The regime separation at 58°S is defined by the maximum seaward extension of the MIZ during the 7 month period.

Measurement-based air-sea fluxes of turbulent latent and sensible heat fluxes and surface radiative fluxes were processed at sea using the COARE algorithm of *Fairall et al*. [2003]. However, the COARE algorithm is

not tuned for applications in the MIZ. The change from the sub-Antarctic open water surface to the MIZ surface that consists of both ice and water creates an abrupt transition in virtually all surface properties, which need to be taken into account in parameterizing the turbulent latent and sensible heat fluxes as well as the surface radiative fluxes. In this study, one major effort was made to reprocess the air-sea flux estimates in the MIZ by utilizing algorithms that are developed for the MIZ. We implemented an area-averaged albedo algorithm of *Brandt et al*. [2005] to account for the effect of sea ice on net solar radiation. We used the SHEBA bulk turbulent flux algorithm of *Andreas et al*. [2010] to estimate the surface fluxes of latent and sensible heat fluxes over the sea-ice margin.

The seasonal variability of air-sea fluxes and the surface energy balance in the Antarctic MIZ and sub-Antarctic Southern Ocean are analyzed. Among all the findings, the most distinct feature is the sea-ice surface modulation of air-sea heat and momentum exchange in the MIZ. Major characteristics are summarized as follows.

1. Wind: Winds over the ice margins were predominantly southerly during the 7 months from October to April. The off-ice air flow experienced a downstream deceleration and convergence within the MIZ, followed by an acceleration and divergence when moving out to the open ocean. The convergence/divergence bands at the ice margins are consistent with previous observations and model results in the Arctic MIZ [*Overland et al*., 1983; *Reynolds*, 1984; *Kantha and Mellor*, 1989], implying that the dynamic adjustments of the ABL to surface roughness are similar in the MIZ of both poles.

2. Air-sea thermodynamical variables: Large fluctuations in air temperature over the MIZ caused the sea-air temperature gradient to vary from positive $4-6$°C in austral spring/fall down to negative 1°C in summer. Hence, the water surface of the MIZ fluxed sensible heat to the atmosphere except for the summer, during which there was a small amount of sensible heat into the ocean. Meanwhile, the air in the MIZ is dry compared to that over the sub-Antarctic Southern Ocean. However, the relative humidity is very high, exceeding 90% most of the time. This phenomenon appears to be ubiquitous in both polar seas, showing that the air over ice is always near saturation [*Persson et al*., 2002; *Andreas et al*., 2002].

3. Surface heat Fluxes: SH had a magnitude similar to LH in the MIZ. Both turbulent fluxes showed marked poleward increase in spring and fall. In the sub-Antarctic, SH was much smaller with magnitude not exceeding 5 W m^{-2}. By comparison, LH was more dominating, increasing equatorward from less than 10 W m^{-2} near the outer edge of the MIZ to greater than 50 W m^{-2} near Hobart. The increase was a result of the increased sea-air humidity gradient.

Within the MIZ, the net SW heat gain at the ocean surface generally decreased toward the pole, while the net LW heat loss at the ocean surface generally increased toward the pole. There is a clear reduction of SW in the MIZ, due primarily to the effect of sea ice on albedo. Of the $\sim$75 W m^{-2} reduction in net solar heating from 45°S poleward to 65°S over October–April, 13 W m^{-2} is due to the sea-ice effect on the change of albedo in the MIZ.

4. Q_{net} and the surface energy budget: Overall, there was a net heat gain in both regimes during the non-winter months, with the net downward SW being the main driver for both seasonal changes and surface budget balance. Compared to the heat budget in the sub-Antarctic, the effect of turbulent heat fluxes, particularly the sensible heat flux, on the MIZ surface heat budget from late summer to Fall (January to April) is worth noting. The monotonic increase of LH and SH during this period balanced out the decreasing net solar heating in the MIZ, turning the MIZ into a net heat loss regime. By comparison, the sub-Antarctic section remained in a net heat gain regime throughout the 7 month period, during which SH was nonsignificant (not exceeding 3 W m^{-2}) and seasonally invariant.

In summary, our analysis has employed a large data set of high-quality shipboard observations to reveal the contrasting air-sea interaction regimes that prevail in the Antarctic MIZ and sub-Antarctic Southern Ocean from austral spring through fall. These observations are highly valuable, showing that the LH and SH are the main cause of the difference in surface heat balance between the two regimes in addition to differences in SW heating. In particular, SH showed more than 1 order of magnitude increase from the sub-Antarctic water to the MIZ during late summer to fall. However, further observations are needed to validate the budget estimates in the MIZ as the sample size acquired by the 22 cruises might be too small. For Q_{net} and SH, the uncertainty estimates that were derived from the standard deviations of the spread in the observations are

larger than or similar to the magnitude of the 7 month mean values. Nevertheless, this study provides a clear formalism to estimate the air-sea turbulent and radiative heat fluxes in the MIZ using the bulk flux algorithms that are tuned for the sea-ice conditions. It allows a first-order insight into the heat and momentum exchanges between the atmosphere and the sea-ice margins in the far Antarctic.

Acknowledgments

L. Yu acknowledges the support of the NOAA Climate Observation Division (COD) grant NA09OAR4320129 for this study. Data were sourced from the Integrated Marine Observing System (IMOS)—IMOS is a national collaborative research infrastructure, supported by Australian Government. We wish to acknowledge the Australian Antarctic Division (AAD) that manages the icebreaker *Aurora Australis* used in the collection of the observations and in making the data accessible from the IMOS website at http://imos.org.au/flux_data.html. NSIDC sea-ice concentration data are downloaded from https://nsidc.org. S. Josey is funded by the UK Natural Environment Research Council. We thank the late Edgar Andreas for providing the FORTRAN code for the SHEBA algorithm at the website http://www.nwra.com/resumes/andreas/.

References

Allison, I. (1989), The East Antarctic sea ice zone: Ice characteristics and drift, *GeoJournal*, *18*, 103–115.

Allison, I., R. E. Brandt, and S. G. Warren (1993), East Antarctic sea ice: Albedo, thickness distribution and snow cover, *J. Geophys. Res.*, *98*, 12,417–12,429.

Anderson, R. J. (1987), Wind stress measurements over rough ice during the 1984 Marginal Ice Zone Experiment, *J. Geophys. Res.*, *92*, 6933–6941.

Andreas, E. L. (1987), A theory for the scalar roughness and the scalar transfer coefficients over snow and sea ice, *Boundary Layer Meteorol.*, *38*, 159–184.

Andreas, E. L., and B. Murphy (1986), Bulk transfer coefficients for heat and momentum over leads and polynyas, *J. Phys. Oceanogr.*, *16*, 1875–1883.

Andreas, E. L., C. A. Paulson, R. M. Williams, R. W. Lindsay, and J. A. Businger (1979), The turbulent heat flux from Arctic leads, *Boundary Layer Meteorol.*, *17*, 57–91.

Andreas, E. L., W. B. Tucker III, and S. F. Ackley (1984), Atmospheric boundary layer modification, drag coefficient, and surface heat flux in the Antarctic marginal ice zone, *J. Geophys. Res. 89*, 649–661.

Andreas, E. L., P. S. Guest, P. O. G. Persson, C. W. Fairall, T. W. Horst, S. R. Semmer, and R. E. Moritz (2002), Near-surface water vapor over polar sea ice is always near ice saturation, *J. Geophys. Res.*, *107*(C10), doi:10.1029/2000JC000411.

Andreas, E. L., T. W. Horst, A. A. Grachev, P. O. G. Persson, C. W. Fairall, P. S. Guest, and R. E. Jordan (2010), Parametrizing turbulent exchange over summer sea ice and the marginal ice zone, *Q. J. R. Meteorol. Soc.*, *136*, 927–943, doi:10.1002/qj.618.

Arya, S. P. S. (1973), Contribution of form drag on pressure ridges to the air stress on Arctic ice, *J. Geophys. Res.*, *78*, 7092–7099, doi:10.1029/JC078i030p07092.

Arya, S. P. S. (1975), A drag partition theory for determining the large-scale roughness parameter and wind stress on the Arctic pack ice, *J. Geophys. Res.*, *80*, 3447–3454, doi:10.1029/JC080i024p03447.

Badgley, F. J. (1966), Heat budget at the surface of the Arctic Ocean, in *Proceedings of the Symposium on the Arctic Heat Budget and Atmospheric Circulation*, edited by J. O. Fletcher, pp. 267–277, Rand, Santa Monica, Calif.

Bauer, J., and S. Martin (1980), Field observations of the Bering Sea ice edge properties during March 1979, *Mon. Weather Rev.*, *108*, 2045–2056.

Bennett, T. J., Jr., and K. Hunkins (1986), Atmospheric boundary layer modification in the marginal ice zone, *J. Geophys. Res.*, *91*, 13,033–13,044.

Birnbaum, G., and C. Lüpkes (2002), A new parameterization of surface drag in the marginal sea ice zone, *Tellus, Ser. A*, *54*, 107–123, doi:10.1034/j.1600-0870.2002.00243.x.

Brandt, R. E., S. G. Warren, A. P. Worby, and T. C. Grenfell (2005), Surface Albedo of the Antarctic Sea Ice Zone, *J. Clim.*, *18*, 3606–3622, doi:10.1175/JCLI3489.1.

Clark, N. E., L. Eber, R. M. Laurs, J. A. Renner, and J. F. T. Saur (1974), Heat exchange between ocean and atmosphere in the eastern North Pacific for 1961–71, *NOAA Tech Rep. NMFS SSFR-682*, 108 pp., U.S. Dep. of Commer., Washington, D. C.

Elvidge, A. D., I. A. Renfrew, A. I. Weiss, I. M. Brooks, T. A. Lachlan-Cope, and J. C. King (2016), Observations of surface momentum exchange over the marginal ice zone and recommendations for its parametrisation, *Atmos. Chem. Phys.*, *16*, 1545–1563, doi:10.5194/acp-16-1545-2016.

Fairall, C. W., and R. Markson (1987), Mesoscale variations in surface stress, heat fluxes, and drag coefficient in the marginal ice zone during the 1983 Marginal Ice Zone Experiment, *J. Geophys. Res.*, *92*, 6921–6932, doi:10.1029/JC092iC07p06921.

Fairall, C. W., E. F. Bradley, J. S. Godfrey, G. A. Wick, J. B. Edson, and G. S. Young (1996), Cool-skin and warm-layer effects on sea surface temperature, *J. Geophys. Res.*, *101*, 1295–1308.

Fairall, C. W., E. F. Bradley, J. E. Hare, A.A. Grachev, and J. B. Edson (2003), Bulk parameterization of air-sea fluxes: Updates and verification for the COARE algorithm, *J. Clim.*, *16*(4), 571–591.

Francis, J. A., and E. Hunter (2006), New insight into the disappearing Arctic sea ice, *Eos Trans. AGU*, *87*(46), 509–511, doi:10.1029/2006EO460001.

Francis, J. A., T. P. Ackerman, K. B. Katsaros, R. J. Lind, and K. L. Davidson (1991), A comparison of radiation budgets in the Fram Strait summer marginal ice zone, *J. Clim.*, *4*, 218–235, doi:10.1175/1520-0442(1991)004 < 0218:ACORBI>2.0.CO;2.

Gordon, A. L., and Ice Station Weddell Group of Principal Investigators and Chief Scientists (1993), Weddell Sea exploration from ice station, *Eos Trans. AGU*, *74*(11), 121–126, doi:10.1029/93EO00260.

Guest, P. S., and K. L. Davidson (1987), The effect of observed ice conditions on the drag coefficient in the summer east Greenland Sea marginal ice zone, *J. Geophys. Res.*, *92*, 6943–6954, doi:10.1029/JC092iC07p06943.

Guest, P. S., J. W. Glendening, and K. L. Davidson (1995), An observational and numerical study of wind stress variations within the marginal ice zone, *J. Geophys. Res.*, *100*, 10,887–10,904.

Hakkinen, S. (1986), Coupled ice-ocean dynamics in the marginal ice zones: Upwelling/downwelling and eddy generation, *J. Geophys. Res.*, *91*, 819–832.

Hellmer, H. H., C. Haas, G. S. Dieckmann, and M. Schroder (2006), Seaice feedbacks observed in western Weddell Sea, *Eos Trans. AGU*, *87*(18), 173–179.

Hill, K. (2010), The Australian Integrated Marine Observing System (IMOS), *Meteorol. Technol. Int.*, *1*, 114–118.

Kantha, L. H., and G. L. Mellor (1989), A two-dimensional coupled ice-ocean model of the Bering Sea marginal ice zone, *J. Geophys. Res.*, *94*, 10,921–10,935, doi:10.1029/JC094iC08p10921.

Katsaros, K. B., L. A. McMurdie, R. J. Lind, and J. E. DeVault (1985), Albedo of a water surface, spectral variation, effects of atmospheric transmittance, sun angle, and wind speed, *J. Geophys. Res.*, *90*, 7313–7321.

Kergomard, C., B. Bonnela, and Y. Fouquart (1993), Retrieval of surface radiative fluxes on the marginal zone of sea ice from operational satellite data, *Ann. Glaciol.*, *17*, 201–206.

Key, J. R., R. A. Silcox, and R. S. Stone (1996), Evaluation of surface radiative flux parameterizations for use in sea ice models, *J. Geophys. Res.*, *101*, 3839–3849, doi:10.1029/95JC03600.
Kottmeier, C., and D. Engelbart (1992), Generation and atmospheric heat exchange of coastal polynyas in the Weddell Sea, *Boundary Layer Meteorol.*, *60*, 207–234.
Liston, G. E., and M. Sturm (2004), The role of winter sublimation in the Arctic moisture budget, *Hydrol. Res.*, *35*(4–5), 325–334.
Martin, S., P. Kauffman, and C. Parkinson (1983), The movement and decay of ice edge bands in the winter Bering Sea, *J. Geophys. Res.*, *88*, 2803–2812,
Maykut, G. A. (1978), Energy exchange over young sea ice in the central Arctic, *J. Geophys. Res.*, *83*, 3646–3658, doi:10.1029/JC083iC07p03646.
Maykut, G. A., and D. K. Perovich (1987), The role of shortwave radiation in the summer decay of a sea ice cover, *J. Geophys. Res.*, *92*, 7032–7044.
McPhee, M. G., G. A. Maykut, and J. H. Morison (1987), Dynamics and thermodynamics of the ice/upper ocean system in the marginal ice zone of the Greenland Sea, *J. Geophys. Res.*, *92*, 7017–7031, doi:10.1029/JC092iC07p07017.
McPhee, M. G., S. F. Ackley, P. Guest, T. P. Stanton, B. A. Huber, D. G. Martinson, J. H. Morison, R. D. Muench, and L. Padman (1996), The Antarctic zone flux experiment, *Bull. Am. Meteorol. Soc.*, *77*, 1221–1232.
Meyers, G. (2008), The Australian integrated marine observing system, *J. Ocean Technol.*, *3*, 80–81.
Miyake, M. (1965), Transformation of the atmospheric boundary layer over inhomogeneous surfaces, Science Report 5R-6, 63 pp., Dep. of Atmos. Sci., Univ. of Wash., Seattle.
Muench, R. D., and R. L. Charnell (1977), Observations of medium-scale features along the seasonal ice edge in the Bering Sea, *J. Phys. Oceanogr.*, *7*, 602–606.
Overland, J. E. (1985), Atmospheric boundary layer structure and drag coefficients over sea ice, *J. Geophys. Res.*, *90*, 9029–9049, doi:10.1029/JC090iC05p09029.
Overland, J. E., R. M. Reynolds, and C. H. Pease (1983), A model of the atmospheric boundary layer over the marginal ice zone, *J. Geophys. Res.*, *88*, 2836–2840.
Persson, P. O. G., C. W. Fairall, E. L. Andreas, P. S. Guest, and D. K. Perovich (2002), Measurements near the Atmospheric Surface Flux Group tower at SHEBA: Near-surface conditions and surface energy budget, *J. Geophys. Res.*, *107*(C10), 8045, doi:10.1029/2000JC000705.
Rao, K. S., J. C. Wyngaard, and O. R. Cote (1974), The structure of the two-dimensional internal boundary layer over a sudden change of surface roughness, *J. Atmos. Sci.*, *31*, 738–746.
Reynolds, M. (1984), On the local meteorology at the marginal ice zone of the Bering Sea, *J. Geophys. Res.*, *89*(C4), 6515–6524, doi:10.1029/JC089iC04p06515.
Ruffieux, D., P. O. G. Persson, C. W. Fairall, and D. E. Wolfe (1995), Ice pack and lead surface energy budgets during LEADEX 1992, *J. Geophys. Res.*, *100*, 4593–4612, doi:10.1029/94JC02485.
Serreze, M. C., J. A. Maslanik, M. C. Rehder, R. C. Schnell, J. D. Kahl, and E. L. Andreas (1992), Theoretical heights of buoyant convection above open leads in the winter Arctic pack ice cover, *J. Geophys. Res.*, *97*, 9411–9422.
Schulz, E., S. A. Josey, and R. Verein (2012), First air-sea flux mooring measurements in the Southern Ocean, *Geophys. Res. Lett.*, *39*, L16606, doi:10.1029/2012GL052290.
Schweiger, A. J., J. Zhang, R. W. Lindsay, and M. A. Steele (2008), Did unusually sunny skies help drive the record sea ice minimum of 2007?, *Geophys. Res. Lett.*, *35*, L10503, doi:10.1029/2008GL033463.
Sedlar, J., M. Tjernstrom, T. Mauritsen, M. D. Shupe, I. M. Brooks, P. O. G. Persson, C. E. Birth, C. Leck, A. Sirevaag, and M. Nicolaus (2011), A transitioning Arctic surface energy budget: The impacts of solar zenith angle, surface albedo and cloud radiative forcing, *Clim. Dyn.*, *37*, 1643–1660.
Smith, P. C., and J. I. MacPherson (1996), Airborne surveys of the atmospheric boundary layer above the marginal ice zone on the Newfoundland shelf, *Atmos.-Ocean*, *34*(1), 161–184, doi:10.1080/07055900.1996.9649561.
Strong, C., and I. G. Rigor (2013), Arctic marginal ice zone trending wider in summer and narrower in winter, *Geophys. Res. Lett.*, *40*, 4864–4868, doi:10.1002/grl.50928.
Untersteiner, N. (1964), Calculation of temperature regime and heat budget of sea ice in the central Arctic, *J. Geophys. Res.*, *69*, 4755–4766.
Vihma, T. (1995), Subgrid parameterization of surface heat and momentum fluxes over polar oceans, *J. Geophys. Res.*, *100*, 22,625–22,646.
Wadhams, P., M. A. Lange, and S. F. Ackley (1987), The ice thickness distribution across the Atlantic sector of the Antarctic Ocean in midwinter, *J. Geophys. Res.*, *92*, 14,535–14,552, doi:10.1029/JC080i013p14535.
Wadhams, P., J. Holfort, E. Hansen, and J. P. Wilkinson (2002), A deep convective chimney in the winter Greenland Sea, *Geophys. Res. Lett.*, *29*(10), 1434, doi:10.1029/2001GL014306.